Nanoscale

Gas-Phase Grafting for the Multifunctional Surface Modification of Silicon Quantum Dots

Journal:	*Nanoscale*
Manuscript ID	NR-ART-09-2022-004902.R2
Article Type:	Paper
Date Submitted by the Author:	10-Nov-2022
Complete List of Authors:	Schwan, Joseph; University of California Riverside, Mechanical Engineering Wang, Kefu; The University of Utah Tang, Ming Lee; The University of Utah, Mangolini, Lorenzo; University of California, Riverside, Mechanical Engineering Deparment, Materials Science and Engineering Program

ARTICLE

Gas-Phase Grafting for the Multifunctional Surface Modification of Silicon Quantum Dots

Received 00th January 20xx,
Accepted 00th January 20xx

DOI: 10.1039/x0xx00000x

Joseph Schwan,[†a] Kefu Wang,[†b,c] Ming Lee Tang*[b,c] and Lorenzo Mangolini*[a,c]

Photon upconversion in systems incorporating inorganic quantum dots (QDs) is of great interest for applications in solar energy conversion, bioimaging, and photodynamic therapy. Achieving high up-conversion efficiency requires not only high-quality inorganic nanoparticles, but also precise control of their surface functional groups. Gas-phase surface functionalization provides a new pathway towards controlling the surface of small inorganic nanoparticles. In this contribution, we utilize a one-step low-temperature plasma technique for the synthesis and in-flight partial functionalization of silicon QDs with alkyl chains. The partially functionalized surface is then modified further with 9-vinylanthracene via thermal hydrosilylation resulting in the grafting of 9-ethylanthracene (9EA) groups. We have found that the minimum alkyl ligand density necessary for quantum dot solubility also gives to the maximum upconversion quantum yield, reaching 17% for silicon QDs with Si-dodecyl chains and an average of 3 9EA molecules per particle.

Introduction

Inorganic nanomaterials functionalized with organic semiconductor molecules are promising candidates for achieving photon upconversion with high efficiency and optical tunability.[1,2] Photon upconversion has potential applications in solar energy harvesting,[3] bioimaging,[4,5] phototherapy,[6,7] and optogenetics.[8,9] In particular, biological applications require that the inorganic nanomaterial is non-toxic, leading to interest in silicon quantum dots (SiQDs).[10] In these systems, the SiQD acts as a photosensitizer and the surface-bound molecules channel the absorbed energy in the form of spin-triplet excitons to an emitter molecule. The emitter molecule supports triplet-triplet annihilation and formation of a spin-singlet excited state, whose decay results in an upconverted photon of shorter wavelength than the absorbed light.[11] This scheme is compatible with a relatively low incident photon flux due to the long lifetime of molecular triplet excitons, 10^{-6} to 10^{-3} seconds.[12] Upconversion quantum efficiencies as high as 15% (with 100% corresponding to 1 upconverted output photon for every 2 input photons) have been recently demonstrated for SiQD systems.[10] However, these high efficiencies require the modification of the nanoparticle surface with molecules with different functionalities. A minimum degree of alkyl chain functionalization is needed to ensure colloidal stability, while an optimal number of transmitter molecules such as acenes need to be grafted onto the surface as well to enable efficient triplet energy transfer. Such multifunctional modification of the silicon surface in a flexible and controllable manner remains challenging. Numerous studies have employed liquid-phase hydrosilylation techniques with and without catalysts to fully functionalize SiQD surfaces with one or more forms of ligand.[13–15] Other techniques like etching of the SiQD itself demonstrate rapid functionalization at the cost of altering the nanocrystal size,[16] however in all of these cases it is difficult to accurately control the relative coverage of alkyl ligands and transmitter molecules on the silicon surface. Liquid-phase techniques may also result in uncontrolled polymerization.[2,10] These limitations demonstrate a clear need for new surface modification strategies that can achieve a complex surface configuration in both a simple and controllable manner.

[a] *Department of Mechanical Engineering, University of California – Riverside, Riverside, California 92521, United States.*
[b] *Department of Chemistry, University of Utah, Salt Lake City, Utah 84112, United States.*
[c] *Materials Science and Engineering Program, University of California – Riverside, Riverside, California 92521, Unit-ed States.*
** Authors to whom correspondence should be sent: lmangolini@engr.ucr.edu, minglee.tang@utah.edu*
† These authors contributed equally.
Electronic Supplementary Information (ESI) available: [details of any supplementary information available should be included here]. See DOI: 10.1039/x0xx00000x

In this contribution, we address this issue by implementing a hybrid gas- and liquid-phase approach. The gas-phase grafting of SiQDs with various organic groups was first introduced by Mangolini and Kortshagen as a way to provide soluble SiQDs immediately after synthesis.[17] Anthony et al. have shown that the same functionalization can be achieved by injecting a gas saturated with an organic ligand in the plasma afterglow, i.e. the region downstream of the powered electrodes where the plasma extinguishes.[18] In this work, alkyl chains are grafted onto the surface of SiQDs immediately after their synthesis in the gas-phase using a low-temperature plasma. Subsequently, 9-vinylanthracene (9VA) is attached to the remaining surface sites via thermal hydrosilylation in mesitylene to form surface bound 9-ethylanthracene (9EA) groups. Here, we show that by carefully controlling the process parameters it is possible to realize partially functionalized SiQDs, i.e. nanoparticles with adequate solubility after in-flight grafting but with unreacted surface sites available for further modification. This approach allows us to investigate how the length and surface density of alkyl chains affects the upconversion with SiQDs. We find that the same solubility can be achieved by grafting roughly 24% of the SiQD's surface with 1-dodecene, in contrast to the 49% coverage of 1-hexene needed, as estimated from FTIR spectra. The partial coverage with Si-dodecyl allows for a greater fraction of the surface to be available for 9EA, whose density can be optimized to maximize the upconversion quantum yield (UCQY). The UCQY is as high as 17.17% when 3 9EA molecules are attached on average per SiQD. On the other hand, only 1.5 9EA molecules can be grafted onto SiQDs with Si-hexyl groups, leading to a lower 5.16% UCQY (see Fig. 1a for cartoon representation). This work provides a new strategy towards achieving SiQDs with a multifunctional surface modification in a rapid, uniform, and tuneable way. This approach simplifies SiQD functionalization and reduces processing time, all while providing material with high upconversion quantum efficiencies. This is highly desirable for the broad range of applications of interest for this novel hybrid organic-inorganic material system.

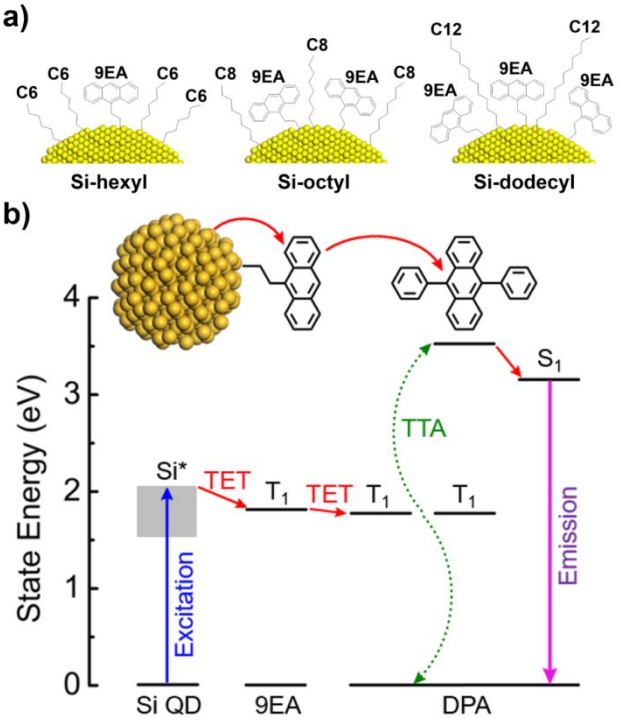

Fig. 1 a) Illustrations of functionalized SiQD with 9EA transmitter ligands and critically loaded alkyl chain ligands to maintain solubility, in addition to b) an energy level diagram illustrating photon upconversion process utilizing TET of the SiQD's photoexcited excitons, through the 9EA, and on to the DPA where they undergo TTA resulting in upconverted photon emission.

Experimental

Upconversion

Photon upconversion is achieved in this hybrid inorganic-organic system through triplet-triplet annihilation (TTA), requiring multiple steps of energy transfer in order to absorb lower and emit higher energy photons.[1] These stages are depicted in Fig. 1b and outline a SiQD being photoexcited to form an exciton. The broad band of energies are due primarily to slight variations in the size of the SiQD.[19] After excitation, the Si exciton transfers to the 9EA transmitter ligand and again transfers via Dexter energy transfer to a nearby 9,10-diphenylanthracene (DPA) molecule in solution. The DPA then collides with a second triplet DPA exciton and undergoes TTA, resulting in one exciton returning to the ground state and the other promoted to a singlet state which in turn fluoresces, emitting a higher frequency 432 nm photon in the process.[2,10] As alluded to earlier, the size of the SiQD and its ability to maintain solubility are extremely sensitive, making the controlled SiQD synthesis and alkyl chain functionalization key to creating an effective upconverting system.

In-flight Synthesis

The first stage of SiQD in-flight synthesis consists of the SiQD formation. A diagram of the in-flight synthesis and partial functionalization system can be seen in Fig. 2. Nanocrystal synthesis is achieved with a low-pressure non-thermal capacitive plasma, contained in a borosilicate reactor with a 5.4 mm internal diameter with energy in the form of strong RF electric fields supplied through 12 mm wide copper loop electrodes. The electrodes are oriented so that the upstream flange is grounded, the live electrode is in the reactor center and downstream is grounded to contain the plasma. The live electrode is powered by a RFPP-RF5S radio frequency (13.56 MHz) generator coupled to the reactor by an MFJ-989D matching network. 30 W of power is applied to a precursor gas mixture of 1.37% (v:v) silane:argon at a flowrate of 60 sccm. The reactor pressure is adjusted to tune particle size through the use of an MKS 253B-1-40-1 exhaust throttle valve placed downstream of both the reactor and the MKS 626D12TBE absolute pressure transducer. An MKS 651CD2S2N digital/analog pressure controller is used to maintain the

reactor pressure at the specified set point. The second stage of the process is the in-flight functionalization of the SiQDs. This is accomplished by flowing hydrogen gas saturated with the ligand into the plasma afterglow. The afterglow environment is sufficiently energetic to drive the grafting of the ligands onto the SiQD surfaces, while avoiding decomposition of the organic ligand. To improve mixing and increase the reaction volume, the reactor is expanded to an inner diameter of 20.5 mm shortly after the downstream grounding electrode while simultaneously injecting the ligand-saturated hydrogen gas through a side inlet. The saturated gas is produced by passing hydrogen through a bubbler filled with the desired ligand. The absolute pressure in the bubbler is kept at 0.1 kPa, 20 kPa, and 100 kPa for the 1-dodecene, 1-octene, and 1-hexene respectively to provide a coarse adjustment of the ligand flow rate. The higher the pressure of hydrogen within the bubbler, the more dilute the ligand's vapor with the hydrogen carrier gas. As a method of fine control, the hydrogen flow through the bubbler is varied between 2.5 and 10 sccm to adjust the flux of ligand molecules entering the plasma afterglow. For consistency in gas flow conditions between samples, additional hydrogen is added downstream of the bubbler so that the total hydrogen flow within the system is 100 sccm. The SiQDs partially functionalized in the gas-phase with aliphatic ligands are transferred air-free into a nitrogen-filled glovebox for further processing.

Liquid Phase Hydrosilylation

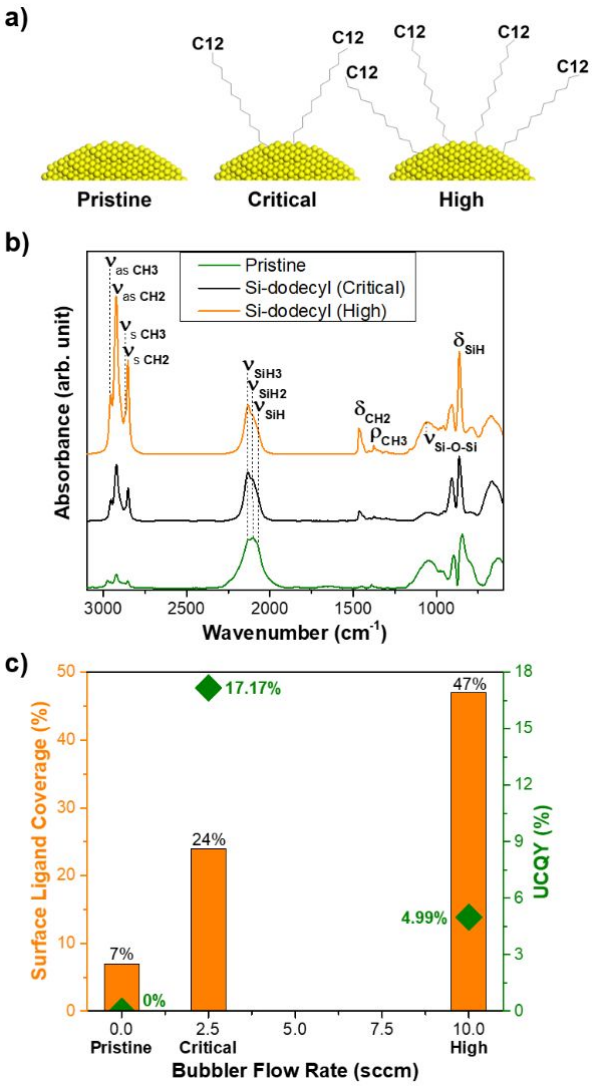

Fig. 3 Three different flow rates of hydrogen gas saturated with 1-dodecene fed to the plasma afterglow alter the SiQD solubility and photon upconversion quantum yield (UCQY). a) Illustrative cartoons of the QD surfaces, b) normalized FTIR spectra for the pristine SiQDs terminated with hydride groups, as well as SiQDs with a critical or high amount of Si-dodecyl ligands. c) The Si-dodecyl chain surface coverage on 3.1 nm diameter SiQDs and their UCQYs plotted against the hydrogen flow rate in the bubbler.

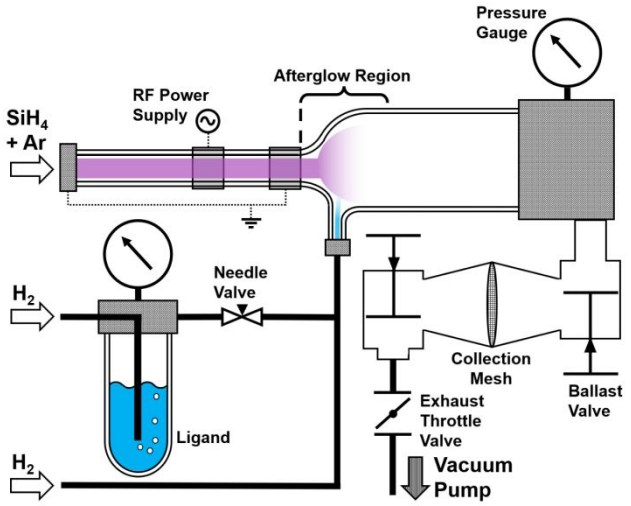

Fig. 2 Simplified diagram of gas-phase SiQD synthesis and in-flight functionalization system using standard electrical and process flow diagram symbols.

The SiQDs partially functionalized with alkyl chains are processed in the glovebox to complete their surface functionalization with transmitter molecules. Samples with no ligands or surface density lower than the critical loading do not disperse to form a clear solution, while materials with a "critical" surface density of alkyl chains form a stable colloidal dispersion in solution (see Fig. 3a for ligand loading illustration and Fig. S1 for sample images illustrating colloidal stability). The thermal hydrosilylation process is then employed with 9VA using published methods as outlined in SI Section 2.2. This method was chosen due to its relative simplicity as a one-step mixing and heating procedure, lack of byproducts, and proven efficacy through previous studies. Upon completion of the hydrosilylation process the functionalized samples are then diluted, placed in 10mm x 10mm path length quartz cuvettes and optically characterized with the same method described by P. Xia et. al.[2]

Sample Characterization

A Thermo Scientific Nicolet iS50 FTIR is used in conjunction with a Pike Technologies ZnSe attenuated total reflectance (ATR) crystal (Catalog #: 1605554) for characterization of the surface chemistry. The material is dispersed in chloroform and dropcast on the ATR crystal. 50 scans are averaged for each measurement from 3100 to 600 cm^{-1} and OMNIC software is used to average the data, remove interference from air and subtract the baseline signal. Using this FTIR absorption spectra in conjunction with absorption cross sections for SiH and the utilized alkyl chain ligands available in the literature, we calculate the approximate ligand surface coverage in percent (SI Section 4).[20,21] Z. Li et al. recently reported that a minimum surface coverage of 25% for Si-octyl on a 3.2 nm diameter silicon particle is needed to maintain solubility, as determined through CHNS elemental analysis. Using the aforementioned FTIR absorbance technique our 3.1 nm diameter Si-octyl functionalized SiQDs require a minimum (aka. critical) surface coverage of 36%, which is consistent with the results from Z. Li et al.[22]

Results and Discussion

Ligand Saturation Effects

We first test the hypothesis that the gas phase functionalization approach can provide control over alkyl ligand surface coverage on SiQDs, and that this in turn affects 9EA grafting and the UCQY. The alkyl chains are grafted to 3.1 nm diameter SiQD first in the gas phase. Then this partially functionalized SiQD undergoes thermally hydrosilylation in solution with 9VA to bind 9EA on the remaining unfunctionalized silicon surface sites. Thus, the surface density of alkyl chains installed in the gas phase allows for control of SiQD functionalization with both ligands. To achieve this, the addition of alkyl chains is controlled by varying the flow rate of hydrogen through a bubbler filled with the terminal alkene ligand. The hydrogen gas becomes saturated by the alkene vapor within the bubbler, so higher flow rates correspond to greater amounts of the alkyl chain being deposited on the SiQD surface. In this study, 0, 2.5, and 10 sccm of hydrogen was flowed through a bubbler filled with 1-dodecene. Part of the sample is analysed with FTIR while the rest is further functionalized with 9EA to investigate the role of Si-dodecyl surface density on the UCQY. The FTIR spectra in Fig. 3b suggest that we can vary the relative magnitudes of the CH_x and SiH_x stretching regions (2700-3050 cm^{-1} and 1900-2300 cm^{-1} respectively) in the Si-dodecyl samples. After normalizing the FTIR data with respect to the absorption cross sections of the surface bound species (outlined in SI Section 4) the ligand surface coverages are shown to vary with bubbler flow rate, (Fig. 3c). For the case of the "pristine sample" (0 sccm of hydrogen through the bubbler) the CH_x peaks present are likely a result of residual 1-dodecene adsorbed to the inner walls of the gas delivery lines. This SiQD sample without any stabilizing Si-dodecyl sediments out of solution and does not show any upconversion. Samples processed with a high flow of 1-dodecene show a reasonable UCQY of 4.99%. An intermediate flow rate of 1-dodecene is needed to maximize the upconversion efficiency at 17.17% (see Fig. S2), as shown in Fig. 3c. This confirms our hypothesis that a precise control of the relative concentrations of alkyl chains and transmitter molecule is needed to optimize optical activity. Note this 17.17% UCQY is currently the highest documented to have been achieved with silicon QD light absorbers for photon upconversion, while relevant QY calculations are shown in SI Section 3.2. We also stress that the triplet exciton transfer from the silicon core to the 9EA group is observed via transient absorption measurement, as shown in Fig. S3.

Next, we compare the optical properties of SiQDs functionalized in-flight with alkyl chains of different lengths: 1-hexene, 1-octene, and 1-dodecene. With longer chains having larger London dispersion interactions, we hypothesize longer alkyl chains will require fewer ligands per SiQD to achieve solubility, thus leaving a greater surface area for attaching the transmitter ligands or further modification as illustrated in Fig. 1a.

Upon finding the critical, or minimum amount of surface bound linear hydrocarbons to attain solubility for 1-hexene and 1-octene, we turn to FTIR to compare the surface density for each alkyl chain. The FTIR data in Fig. 4a indicates that the ratio of CH_x with respect to SiH_x peaks slightly decrease as the alkyl chain length increases. Calculation of the ligand surface coverage demonstrates that increased consumption of nanoparticle surface area by shorter alkyl chains is needed to ensure solubility, as shown in Fig. 4b. To confirm this relation, the SiQD surface is saturated in these samples to occupy the remaining available surface sites with 9EA. Using UV-vis absorption measurements, we are able to determine the average number of surface bound 9EA, with the calculation method available in SI Section 3.1. This number correlates directly with the available surface area on the SiQD after gas phase alkyl functionalization, and inversely with alkyl chain surface coverage, as shown in Fig. 4b and Fig. 4c. This is to say, samples functionalized in-flight with the longer chain 1-dodecene require fewer surface-bound aliphatic chains to maintain solubility. Thus, these SiQDs have more available surface area permitting a higher number of 9EA groups per particle compared to SiQDs with shorter chains.

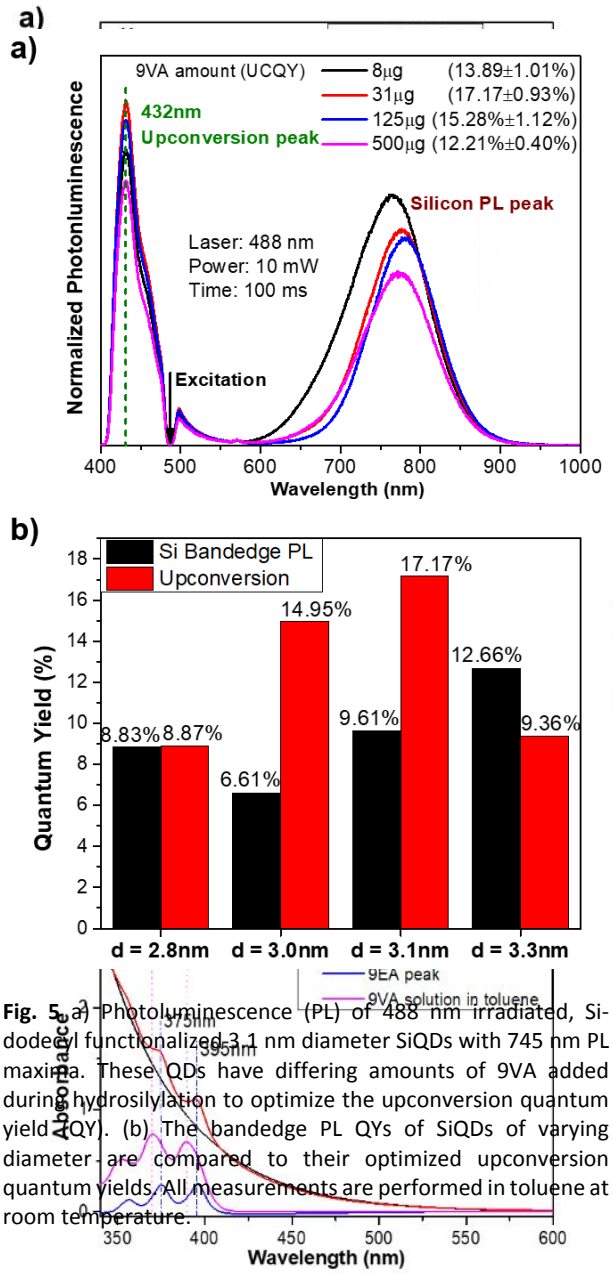

Fig. 5 a) Photoluminescence (PL) of 488 nm irradiated, Si-dodecyl functionalized 3.1 nm diameter SiQDs with 745 nm PL maxima. These QDs have differing amounts of 9VA added during hydrosilylation to optimize the upconversion quantum yield (QY). (b) The bandedge PL QYs of SiQDs of varying diameter are compared to their optimized upconversion quantum yields. All measurements are performed in toluene at room temperature.

Fig. 4 Prior to affixing the 9EA transmitter ligands to the SiQDs, the minimum amount of aliphatic ligands required to maintain solubility in toluene (critical loading) is investigated with 1-dodecene, 1-octene, or 1-hexene. a) Normalized FTIR scans of the partially functionalized SiQDs, which provide the b) Alkyl chain surface coverage on the SiQDs vs. the average number of surface-bound 9EA per SiQD after 9VA hydrosilylation. c) UV-Vis absorption spectra showing 9EA is bound to the SiQD surface.

Size Effects

Previous sections investigate the control of SiQD surface coverage while manipulating alkyl chain length for SiQDs of size ~3.1 nm. Semiconducting nanomaterial size influences bandgap and exciton energy.[19,23] As a result, we hypothesize that both bandedge photoluminescence energy and the UCQY will be directly impacted by the absorber size. To investigate this, the absolute pressure in the low-temperature plasma reactor is varied between 0.7 and 1 Torr. The reactor pressure affects residence time and plasma characteristics, in turn affecting particle size, with higher pressure leading to larger SiQDs. Using the pressure control system described in the In-flight Synthesis section to control reactor pressure, the average SiQD diameter can be shifted from 2.8 to 3.3 nm. The reported particle sizes are estimated from the peak bandedge PL wavelength using data from Wheeler et al.[24] These SiQDs are partially functionalized with dodecyl using identical mass flow rates of dodecene-saturated hydrogen for consistency. The samples of partially functionalized SiQDs with differing diameters then undergo hydrosilylation with 9EA. As shown in Fig. 5a, differing amounts of 9VA are used in the hydrosilylation process to control the surface density of 9EA to find the maximum UCQY of a sample (Table S2). Fig. 5b shows that the maximum UCQY occurs for the 3.1 nm diameter sample with a sharp drop off in as the particle diameter either increases or decreases. Additionally, bandedge PL appears to overtake upconversion only when the SiQD diameter is greater than the optimum (PL QY calculations are shown in SI Section 3.3). A UCQY of 17.17% is measured for the 3.1 nm diameter sample with a corresponding PL peak of 745 nm. The observed phenomenon that UCQY of SiQDs increases with size, then decreases after an

optimal diameter can be explained by the balance between the driving force for triplet energy transfer from the SiQD to the surface 9EA and the QD exciton lifetime. As SiQDs increase in size, it is expected that the exciton lifetime increases due to the reduced confinement of a larger crystal volume, which in turn reduces exciton recombination probability. A longer QD donor lifetime promotes energy transfer to the 9EA acceptors.[25] However, the triplet exciton energy decreases as SiQD size increases leading to a smaller driving force for triplet transfer from the SiQD to the 9EA. Reduction of exciton energy due to increased SiQD size is a result of the dependence of a semiconducting material's energy gap and auger rate on its size, with smaller diameters leading to higher energy gaps and a greater triplet transfer driving force.[19] When exciton energy from the SiQD begins falling below the 9EA triplet energy, a smaller fraction of excitons undergoes energy transfer between the crystal and the transmitter ligand. Consequently, a reduced population of excitons can diffuse to the 9EA, resulting in a smaller driving force and a reduced photon upconversion efficiency for larger SiQDs.[23,26] Thus, an optimal size is to be expected and is consistent with the observed results. We point out that the UCQY is reproducible within ±1.1% and the band edge PL QY within ±0.8%, confirming that the trends observed here are statistically significant.

Alkyl Chain Ligand:UCQY Relation

Finally, we provide a more detailed analysis of the fraction of the surface covered with various alkyl groups, for the conditions that maximize UCQY. Using the bulk density of silicon, we calculate that a 3.1 nm SiQD has ~780 total atoms, with between 204 and 290 of them being at the particle surface (see SI Section 5). The much higher surface coverage of 1-hexyl groups (49%) compared to Si-dodecyl groups (24%) is consistent with fewer surface sites available for the 9EA transmitter ligand for the case of Si-hexyl as shown in Fig. 4b, which is in turn consistent with the reduction in UCQY shown in Fig. 6a. Aggregating these observations, in Fig. 6b we show that the ligand length does not appear to affect UCQY directly. This is demonstrated by comparing the Si-dodecyl sample with increased hydrogen flow rate through the bubbler so that the fraction of surface covered with Si-dodecyl (47%) is reasonably close to the fraction covered by Si-hexyl (49%). When 9VA is grafted onto the remaining surface sites of both, a very similar UCQY is measured between 12-carbon and 6-carbon long functionalization (5% for Si-dodecyl and 5.2% for Si-hexyl). It is not the length of the alkyl chain that limits the UCQY, but rather the availability of surface site for 9VA grafting.

Conclusions

This work shows that a gas-phase approach to surface modification allows for consistent and independent control over the type of ligand grafted onto SiQDs and its degree of surface coverage. The produced materials are readily soluble immediately after collection from the gas-phase reactor, simplifying any additional solution-based surface modification that is required to achieve the desired functionality. We find that it is preferable to utilize longer alkyl chains (Si-dodecyl vs. 1-hexyl) to attain solubility with a low aliphatic ligand surface coverage (~24% vs. ~49%), as this allows the grafting of 9EA transmitter ligands to ensure efficient energy transfer with DPA and a resulting high UCQY (17.17% vs. 5.16%). We also conclude that the length of optoelectronically inactive ligands does not impact the upconversion process per se, but rather it affects the ability to further functionalize the surface with transmitter molecules. While our approach specifically focuses on optical upconversion, the same functionalization strategy is likely desirable for other applications. For instance, hybrid organic-inorganic light emitting diodes, printed transistors or solar cells require building blocks with both good solubility for processability reasons and good electronic contact between the particles and the organic matrix for optimal functionality. The approach described here is a route towards such materials.

Author Contributions

The manuscript was written through contributions of all authors. All authors have given approval to the final version of the manuscript.
† Joseph Schwan and Kefu Wang contributed equally.

Conflicts of Interest

There are no conflicts to declare.

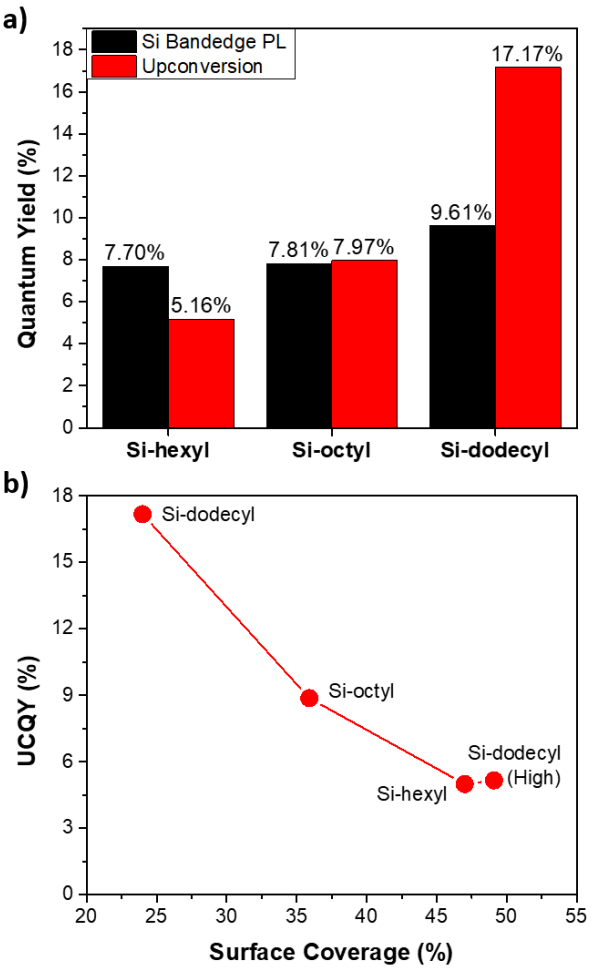

Fig. 6 a) The bandedge photoluminescence and upconversion quantum yields for 3.1 nm diameter SiQDs functionalized with critical surface density of Si-hexyl, Si-octyl and Si-dodecyl, i.e. the minimum amount of aliphatic ligands required for colloidal stability. b) Comparison between ligand surface coverage and UCQY showing similar rates of surface coverage produce similar UCQY.

Acknowledgements

The authors acknowledge the support of the US National Science Foundation (NSF) via grant number 2053567.

Notes and References

1 Z. Huang, X. Li, M. Mahboub, K. M. Hanson, V. M. Nichols, H. Le, M. L. Tang and C. J. Bardeen, *Nano Lett.*, 2015, **15**, 5552–5557.

2 P. Xia, E. K. Raulerson, D. Coleman, C. S. Gerke, L. Mangolini, M. L. Tang and S. T. Roberts, *Nat. Chem.*, 2020, **12**, 137–144.

3 H. Lu, Z. Huang, M. S. Martinez, J. C. Johnson, J. M. Luther and M. C. Beard, *Energy Environ. Sci.*, 2020, **13**, 1347–1376.

4 T. Jia, Q. Wang, M. Xu, W. Yuan, W. Feng and F. Li, *Chem. Commun.*, 2021, **57**, 1518–1521.

5 X. Liang, J. Fan, Y. Zhao and R. Jin, *J. Rare Earths*, 2021, **39**, 579–586.

6 M. Huo, P. Liu, L. Zhang, C. Wei, L. Wang, Y. Chen and J. Shi, *Adv. Funct. Mater.*, 2021, **31**, 1–10.

7 X. Chen, Y. Zhang, X. Zhang, Z. Zhang and Y. Zhang, *Microchim. Acta*, , DOI:10.1007/s00604-021-04915-w.

8 Y. Zhai, Y. Zhou, X. Yang, F. Wang, W. Ye, X. Zhu, D. She, W. D. Lu and S. T. Han, *Nano Energy*, 2020, **67**, 104262.

9 S. Chen, A. Z. Weitemier, X. Zeng, L. He, X. Wang, Y. Tao, A. J. Y. Huang, Y. Hashimotodani, M. Kano, H. Iwasaki, L. K. Parajuli, S. Okabe, D. B. Loong Teh, A. H. All, I. Tsutsui-Kimura, K. F. Tanaka, X. Liu and T. J. McHugh, *Science (80-.).*, 2018, **359**, 679–684.

10 P. Xia, J. Schwan, T. W. Dugger, L. Mangolini and M. L. Tang, *Adv. Opt. Mater.*, 2021, **9**, 1–6.

11 S. Singh, W. J. Jones, W. Siebrand, B. P. Stoicheff and W. G. Schneider, *J. Chem. Phys.*, 1965, **42**, 330–342.

12 M. Montalti, A. Credi, L. Prodi and M. T. Gandolfi, *Handbook of Photochemistry*, 3rd edn., 2006.

13 M. Villa, S. Angeloni, A. Bianco, A. Gradone, V. Morandi and P. Ceroni, *Nanoscale*, 2021, **13**, 12460–12465.

14 G. M. Carroll, R. Limpens and N. R. Neale, *Nano Lett.*, 2018, **18**, 3118–3124.

15 C. M. Hessel, D. Reid, M. G. Panthani, M. R. Rasch, B. W. Goodfellow, J. Wei, H. Fujii, V. Akhavan and B. A. Korgel, *Chem. Mater.*, 2012, **24**, 393–401.

16 M. H. Mobarok, T. K. Purkait, M. A. Islam, M. Miskolzie and J. G. C. Veinot, *Angew. Chemie - Int. Ed.*, 2017, **56**, 6073–6077.

17 L. Mangolini and U. Kortshagen, *Adv. Mater.*, 2007, **19**, 2513–2519.

18 R. J. Anthony, K. Y. Cheng, Z. C. Holman, R. J. Holmes and U. R. Kortshagen, *Nano Lett.*, 2012, **12**, 2822–2825.

19 I. Robel, R. Gresback, U. Kortshagen, R. D. Schaller and V. I. Klimov, *Phys. Rev. Lett.*, 2009, **102**, 1–4.

20 P. Gupta, V. L. Colvin, J. L. Brand and S. M. George, 2008, **50**, 50–59.

21 A. E. Klingbeil, J. B. Jeffries and R. K. Hanson, *J. Quant. Spectrosc. Radiat. Transf.*, 2007, **107**, 407–420.

22 Z. Li and U. R. Kortshagen, *Chem. Mater.*, 2019, **31**, 8451–8458.

23 D. Jurbergs, E. Rogojina, L. Mangolini and U. Kortshagen, *Appl. Phys. Lett.*, , DOI:10.1063/1.2210788.

24 L. M. Wheeler, N. C. Anderson, P. K. B. Palomaki, J. L. Blackburn, J. C. Johnson and N. R. Neale, *Chem. Mater.*, 2015, **27**, 6869–6878.

25 M. Mahboub, Z. Huang and M. L. Tang, *Nano Lett.*, 2016, **16**, 7169–7175.

26 T. Huang, T. T. Koh, J. Schwan, T. T. T. Tran, P. Xia, K. Wang, L. Mangolini, M. L. Tang and S. T. Roberts, *Chem. Sci.*, 2021, **12**, 6737–6746.